Code-to-Code Nonlinear Hydrodynamic Modelling Verification for Wave Energy Converters: WEC-Sim vs. NLFK4ALL

Giuseppe Giorgi, Markel Penalba, and Rui P.F. Gomes

***Abstract*—In the wave energy conversion field, simulation tools are crucial for effective converter and controller design, but are often prone to become very case-specific, in both structure and parameter selection. This is due to majorly different working principles and diverse importance of nonlinear effects, at times requiring ad-hoc modelling approaches. To tackle this challenge, WEC-Sim (Wave Energy Converter SIMulator) was born from the National Renewable Energy Laboratory (NREL) and Sandia National Laboratories, providing a unique simulation platform for all WECs. Nonlinearities related to time-varying wetted surface, especially important in floating WECs, are included in WEC-Sim through a mesh-based computation of nonlinear Froude-Krylov forces. Virtually arbitrary geometries can be considered, thanks to the discretized representation of wetted surfaces, at the price of a significant increase in computational burden. This paper considers a time-effective alternative, implemented in the open-source toolbox called NLFK4ALL, applicable to the popular and wide family of axisymmetric floaters. The Spar-buoy floating oscillating water column device is considered, particularly challenging due to a submerged volume composed of several different sections. The accuracy of WEC-Sim and NLFK4ALL is verified by a preliminary cross-comparison, using independent methods to compute virtually same effects. Fixed-body numerical experiments are used to quantify nonlinearities and compare not only the accuracy, but also the computation burden. Results show that both methods provide almost identical results, although WEC-Sim doubles computational requirements.**

***Index Terms*—Wave Energy Converters Nonlinear Froude-Krylov force, Spar-buoy oscillating OWC, WEC-Sim, NLFK4ALL.**

I. Introduction

SIMULATION tools are essential for effective design and development of power conversion systems. However, the definition of a reliable and representative mathematical model for wave energy converters (WECs) is especially challenging. In fact, there is a wide variety of devices, based on substantially different working principles and mounting various components, often making the model quite case-specific. Moreover, since an appropriate representation of nonlinear effects is likely to be required for achieving acceptably accurate results, the complexity of mathematical models rapidly escalates, at the expense of its transparency and flexibility [1]. In order to address such issues, the National Renewable Energy Laboratory (NREL) and Sandia National Laboratories developed the open source high-level software in 2014 WEC-Sim (Wave Energy Converter SIMulator) [2]. WEC-Sim is gaining increasing popularity in the wave energy community, both academic and industrial, since it provides a framework for simulating virtually any WEC [3], including different subsystems of the wave energy conversion chain: from mooring systems [4] to power take-off [5], including various nonlinear hydrodynamic effects [6]. This paper focuses especially on the computation of the nonlinear Froude-Krylov (NLFK) force, which is one of the major and most impactful nonlinearity in floating WECs [7]–[9], with effects on parametric resonance [10], [11], mooring design [12] and model-based controller design [13], [14]. NLFK forces are due to the undisturbed pressure field acting on the instantaneous wetted surface of the floater, whereas the linear approximation considers the mean wetted surface as constant. Geometries of arbitrary complexity require a mesh-based discretization of the wetted surface, that can be handled in two alternative ways: either a re-meshing routine is used, re-computing the mesh discretization at each time step according to the instantaneous position of the floater with respect to the free surface elevation; or a constant but very fine mesh is implemented, with a boolean decision on which panel is either fully wet or fully dry [15]. Both approaches may slow down the simulation significantly, depending on the size of the spatial discretization. WEC-Sim, with the purpose of being flexible on the floater shape, implements a mesh-based computation of NLFK forces [16]. However, for axisymmetric geometries there is an equivalent but computationally more efficient approach based on an analytical formulation of the instantaneous wetted surface, hence getting rid of the computational bottleneck of the meshed wetted surface [17]. An additional frequency-domain (FD) approach was also suggested in [18], where nonlinear effects are included using a projection of the dynamical equations onto a basis of trigonometric functions.

Note that the popular family of point absorber WECs is mainly composed of axisymmetric devices, making such an assumption not too restrictive. Therefore, the analytical approach, available in the open source Matlab demonstration toolbox NLFK4ALL [19] and

This research was funded by the European Research Council (ERC) under the European Unions Horizon 2020 research and innovation programme under Grant Agreement No. 832140

Marine Offshore Renewable Energy Lab (MOREnergy Lab), DIMEAS, Politecnico di Torino, Corso Duca degli Abruzzi 24, 10129, Turin, Italy (e-mail: giuseppe.giorgi@polito.it).

Department of Mechanical and Manufacturing, Mondragon University, Loramendi 4 Apdo. 23, 20500, Arrasate, Spain (e-mail: mpenalba@mondragon.edu).

IDMEC, Instituto Superior Técnico, Universidade de Lisboa, Av. Rovisco Pais 1, 1049-001 Lisboa, Portugal (e-mail: ruigomes@tecnico.ulisboa.pt).

 Copyright © European Wave and Tidal Energy Conference 2021

validated with experimental wave tank data [20], is implemented in this paper, and compared with results obtained with the nonlinear hydrodynamics features of WEC-Sim. The existing Sparbuoy floating oscillating water column (OWC) is used as a case study [21].

The reminder of the paper is organized as follows: Sect. II introduces the device considered in this paper, used to quantify the comparison between the two proposed approaches for the NLFK calculation, WEC-Sim and NLFK4ALL, respectively discussed in Sect. II-B and Sect. II-C. Section III shows results, while some final remarks and conclusions are provided in Sect. IV.

II. The Spar-buoy OWC device

The Spar-buoy OWC is a floating oscillating water column, composed of a hollow floater opened at the bottom, hence containing a water column within its structure. As waves arrive, a relative motion between the floater and the water column is generated, driving the air pocket above the water column through a turbine, extracting useful energy. Figure 1 shows a picture of the prototype [22], tested at 1:16 scale. This device, being of the spar buoy type, is prone to experience the highly nonlinear phenomenon of parametric resonance: when the excitation frequency is twice that of the natural frequency of the pitching degree of freedom (DoF), the system becomes parametrically unstable and diverts part of the incoming energy to the rolling DoF [23]. Such a behaviour, potentially detrimental for power extraction efficiency and hindering survivability, is due to time-variations of the wetted surface, so that it can be successfully articulated by NLFK models. For this reason, the Spar-buoy is an appropriate choice for the case study presented in this paper.

Fig. 1. 1:16 scale prototype of the Spar-buoy OWC is a floating oscillating water column [22].

A. Nonlinear Froude-Krylov force

Froude-Krylov forces are defined as the integral of the undisturbed pressure field (p) over the wetted surface of the floater. In the linear approximation, it is assumed that the relative motion between the body and the free surface is small, so that FK forces are computed with respect to the mean wetted surface. On the contrary, nonlinear FK force calculations are performed with respect to the actual *instantaneous* wetted surface ($S_w(t)$):

$$\mathbf{f}_{FK} = \mathbf{f}_g + \iint_{S_w(t)} p\mathbf{n}\, dS, \tag{1a}$$

$$\boldsymbol{\tau}_{FK} = \mathbf{r}_g \times \mathbf{f}_g + \iint_{S_w(t)} p\mathbf{r} \times \mathbf{n}\, dS, \tag{1b}$$

where $\mathbf{f}_{FK}$ are nonlinear forces, $\boldsymbol{\tau}_{FK}$ are torques, $\mathbf{f}_g$ is the gravity force, $\mathbf{n}$ is the unity vector normal to the surface, $\mathbf{r}$ is the generic position vector, and $\mathbf{r}_g$ is the position vector of the centre of gravity. The undisturbed incident pressure field of an uni-directional regular wave travelling in the x-direction is defined as:

$$p(x,z,t) = -\rho g \left[z + a\cos(\omega t - kx)\, \frac{\cosh(k(z'+h))}{\cosh(kh)} \right], \tag{2}$$

where a, ω, and k are the wave amplitude, frequency, and wavenumber, respectively, ρ the water density, g the acceleration of gravity, h the water depth, and z' the vertical coordinate z modified according to Wheeler's stretching [24]:

$$z' = h\frac{z+h}{\eta+h} - h \tag{3}$$

where η is the free surface elevation.

B. The WEC-Sim mathematical model

The WEC-Sim mathematical model is based on a Simulink implementation [2], with specifically designed blocks for typical components of wave energy converters. Figure 2 shows a snapshot of the block diagram for the Spar-buoy, with two hydrodynamic bodies, respectively the floater and the OWC, between which there is a translational power take-off (PTO) unit converting the relative motion into electricity. The system is then referenced to the global-frame through a constraint block, which can be set to free motion (6-DoF), planar motion (3-DoF), vertical motion (1-DoF), or no motion (fixed).

The PTO system of an OWC is an air turbine, which converts the bidirectional air flow induced by the OWC motion inside the floater. The pressure drop across the turbine can be simulated at model scale using an orifice plate [21]:

$$F_{PTO} = \frac{8\rho_a A_a^3}{\pi^2 C_d^2 d_0^4} \dot{z}_r |\dot{z}_r| \tag{4}$$

where ρ_a is the air density, A_a is the cross-sectional area of the air chamber, C_d is the discharge coefficient ($C_d =$

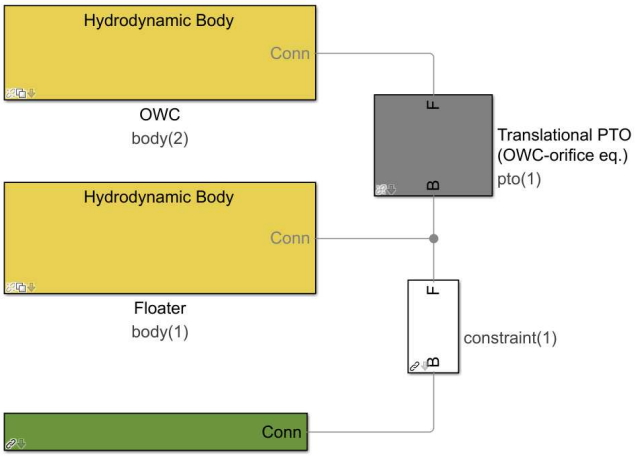

Fig. 2. Simulink block diagram in WEC-Sim.

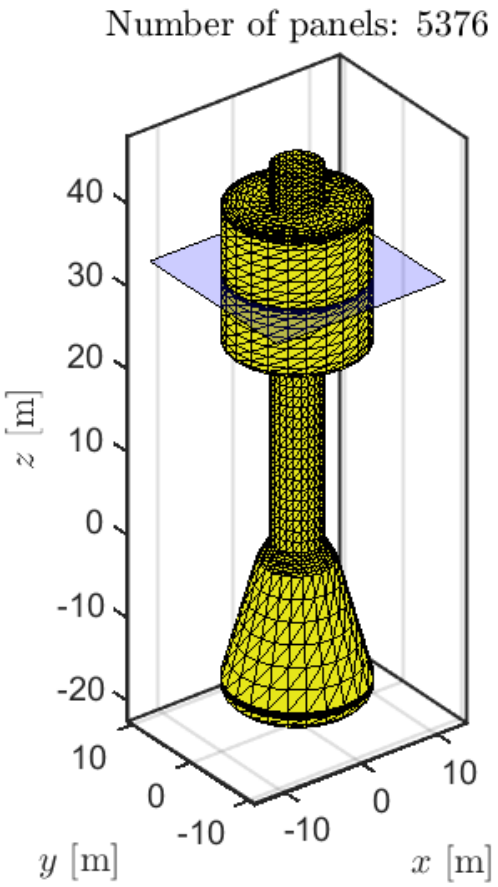

Fig. 3. Mesh discretization of the Spar-buoy device, used for both the BEM code for the linear hydrodynamic curves, and for the NLFK computation in WEC-Sim.

0.6466 for the orifice plate used in the experiments), d_0 is the diameter of the orifice plate, and $\dot{z}_r$ is the relative velocity between the water column and the buoy. Note that F_{PTO} acts on both the buoy and the water column, but with opposite sign.

The NLFK calculations in WEC-Sim (NLFK$_s$) are performed based on a panel mesh, summing up all the contribution of each mesh panel. The mesh used in this study, shown in Fig. 3, has been used for both the NLFK calculation and computation of FD hydrodynamic coefficients via the boundary element method (BEM) software WAMIT [25]. The computational time and accuracy of the NLFK$_s$ approach are highly dependent on the number and size of panels, respectively. The mesh considered in this study is composed of 5376 panels.

C. The NLFK4ALL mathematical model

While solving the integrals in (1) requires, in general, mesh-based approaches, a computationally efficient approach is available for axisymmetric bodies, exploiting cylindrical coordinates (ϱ, ϑ) to achieve an analytical representation of the wetted surface:

$$\begin{cases} \hat{x}(\varrho,\vartheta) = f(\varrho)\cos\vartheta \\ \hat{y}(\varrho,\vartheta) = f(\varrho)\sin\vartheta \\ \hat{z}(\varrho,\vartheta) = \varrho \end{cases} \quad , \quad \vartheta \in [-\pi,\pi) \wedge \varrho \in [\varrho_1,\varrho_2] \quad (5)$$

where $f(\varrho)$ is a generic function of the vertical coordinate ϱ, describing the profile of revolution of the axisymmetric body. Since it is convenient to define the FK integrals in the body-fixed frame of reference, the pressure field must be mapped from the global to the body-fixed frame. After the required adjustments, the integral in (1a), for example, becomes:

$$\begin{aligned} \mathbf{f}_{FK} &= \mathbf{R}_{\boldsymbol{\Theta}}^T \mathbf{f}_g + \iint_{S_w(t)} P(\hat{x},\hat{y},\hat{z})\ \mathbf{n}\ dS = \\ &= \mathbf{R}_{\boldsymbol{\Theta}}^T \mathbf{f}_g + \int_{-\pi}^{\pi}\int_{\varrho_1}^{\varrho_2} P(\varrho,\vartheta)\,(\mathbf{e}_\varrho \times \mathbf{e}_\vartheta)\ d\varrho\ d\vartheta, \end{aligned} \quad (6)$$

where $\mathbf{R}_{\boldsymbol{\Theta}}$ is the rotation matrix from body- to world-frame, $\mathbf{e}_\varrho$ and $\mathbf{e}_\vartheta$ are the unit vector along ϱ and ϑ, respectively. Note that when internal patches (facing the water column) are considered, the sign of the normal vector in (6) should be reversed. The integral in (6) is solved numerically, using a 2D-quadrature scheme for trapezoidal integration [26]. An open source Matlab demonstration toolbox for definition and computation of nonlinear FK forces for axisymmetric floaters is available at [19].

Fig. 4 shows, for an arbitrary displacement of the buoy and wave field, the configuration in both the world-frame (on the left) and the body-frame (on the right), and the corresponding mapping of the free surface elevation. Note that the mesh-like representation in Fig. 4 has a mere visualization purpose, since the surfaces are described analytically and no mesh is needed.

Note that the considered geometry is rather complex, with several changes of cross-sectional area. Twelve different patches can be identified, namely 5 cylindrical sections, 4 conical sections, 2 quarters of torus, and a disk for the inner piston. This increases the overall computational time, since each patch requires an independent formulation, hence raising the number of integrals to be computed. However, it is worth remarking that equally considering all patches is likely to be unnecessary, since some patches are relatively

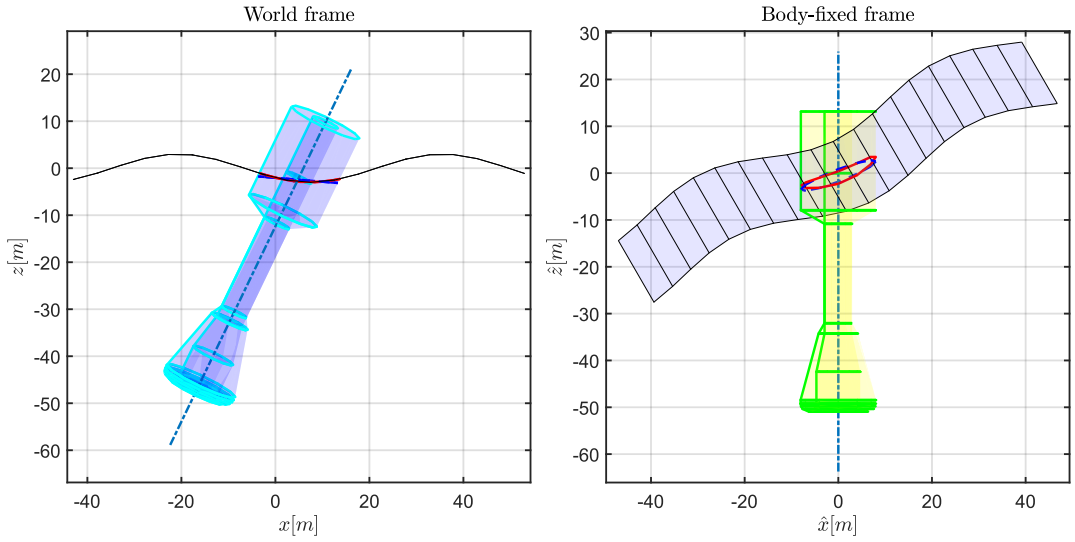

Fig. 4. Example of displaced buoy, in the world frame (on the left) and body-fixed frame (on the right), with corresponding mapped wave field and its intersection with the buoy.

small and/or so deep that the dynamic pressure has already significantly decayed. Nevertheless, since the purpose of this paper is comparison rather than computational time minimization, no simplifying assumption has been investigated.

III. Results

While WEC-Sim naturally provides a framework for time-simulations, the analytical-based NLFK computation algorithm (NLFK_a) has been included into an in-house code. The correctness of implementation is verified via comparison of time-domain simulations (TD) for small (linear) waves, independently computed with WEC-Sim and the in-house code, compared with linear frequency domain (FD) simulations. Figure 5 shows the resulting response amplitude operator (RAO) in surge, heave, and pitch, for a representative set of wave periods (T_w) at a wave height (H_w) of 0.25m. A perfect overlap is obtained between all models, giving confidence on the flawless implementation of the time-domain models under linear conditions.

Successively, in order to ease the comparison between NLFK_a and NLFK_s, results are generated for a numerical excitation force experiment, i.e. by fixing the floater at the rest position, and sending monochromatic waves, at different T_w and H_w; the total excitation force is measured, composed of NLFK and linear diffraction components. While the proportionality between linear forces and H_w is constant for all the the range of H_w, nonlinear forces may show differences as H_w increases.

A. Computational time

Quantifying the computational time has important consequences on the applicability of either of the two models for specific simulation purposes, ranging from power production, response and load assessment, to control and optimization. However, since both accuracy and computational effort depend on different setup parameters for each model, a comprehensive sensitivity analysis should be performed in order to express a definitive, robust and solid statement on the comparative performance.

Calculations are performed on a single core of a standard laptop, with processor Intel(R) Core (TM) i7-7500U CPU @ 2.70GHz and 8GB RAM. Since the overall computational effort depends on the time-advancing scheme and time step size (δt), the computational time is hereafter referred to a single time step execution of the numerical excitation force experiment (t_{CPU}). WEC-Sim results in a required 6 ms per δt, which seems satisfactory. However, the excitation force experiment is favourable to mesh-based approaches, since the mesh is not displaced at each time step, which may increase the computational time. Moreover, with the current mesh discretization, the accuracy of NLFK_s is questionable in surge and pitch for longer waves, as further discussed in Sect. III-B; therefore, a more refined mesh should be tested, implying higher computational burden. Nevertheless, it can be assumed with confidence that the computational time for NLFK_s remains, at worst, below the tens of milliseconds per δt, which is faster than previous mesh-based approaches suggested in the literature, *e.g.* [15].

Conversely to the NLFK_s approach, the considered case study of the Spar-buoy is particularly disadvantageous to the NLFK_a approach. In fact, the computational time is linearly proportional to the number of geometrical sections considered; therefore, NLFK force computation for the Spar-buoy, composed of 12 patches, is likely to be about 3 times longer than the time required for a simpler floater composed of just 4 patches (for example 2 cylinders connected via a truncated cone). Nevertheless, the resulting computational time is of about 3 ms per δt.

B. NLFK results

Figure 6 shows a representative time trace of the total excitation force (Froude-Krylov and diffraction), using the linear model (LFK) as a reference benchmark, and the nonlinear models for comparison. Since they

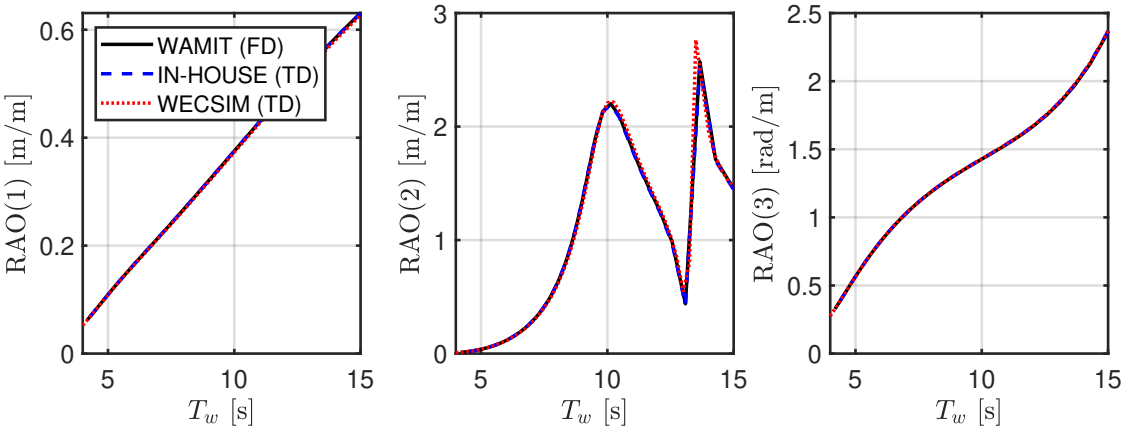

Fig. 5. Response amplitude operators (RAO) in surge (left), heave (middle), and pitch (right), using linear frequency domain (FD) data, and time-domain (TD) models with a small wave (height of 0.25m).

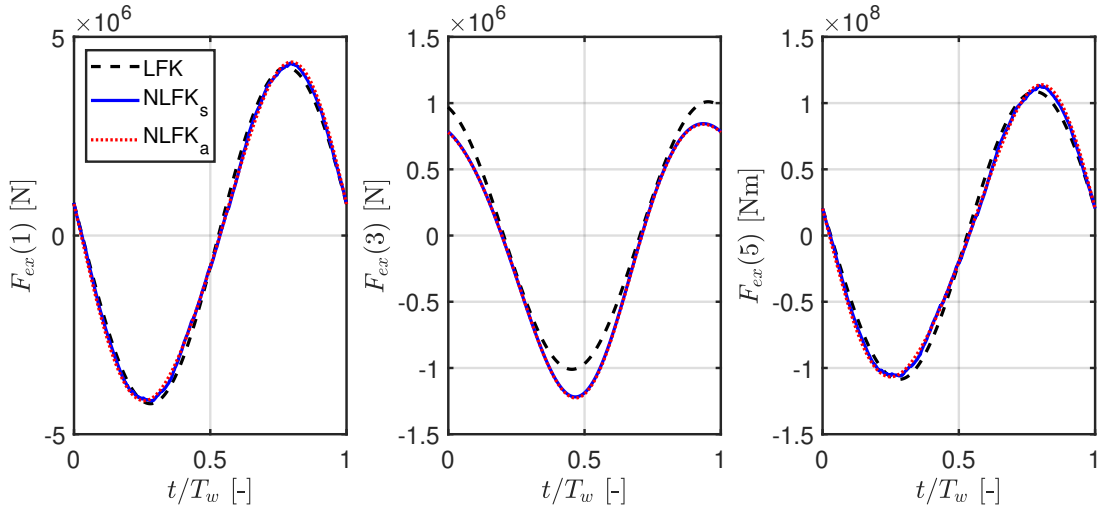

Fig. 6. Time trace over a single wave period of the total excitation force at T_w of 7 s and H_w of 4 m.

are different approaches to compute the same quantity, they should overlap. In Fig. 6 a short wave T_w of 7 s is considered, with H_w of 4 m, hence very steep and nonlinear. It can be remarked that NLFK$_s$ and NLFK$_a$ agree well, particularly in heave. Differences between linear and nonlinear forces are negligible in surge and pitch, while are remarkable in heave.

Figure 7 shows a long wave, T_w of 14 s, at the same height of 4 m. On the one hand, the perfect match between NLFK approaches is preserved in heave; on the other hand, NLFK$_s$ presents irregular oscillation in surge and pitch due to numerical inaccuracies, while NLFK$_a$ remains smooth. This can be ascribed to a static mesh-discretization of the wetted surface, not sufficiently refined to describe variations of the nonlinear forces smoothly. In fact, although very wobbly, the moving average of NLFK$_s$ follows the NLFK$_a$ trend closely. The numerical inaccuracies of NLFK$_s$ are not present in heave because the portion of the buoy intersecting the free surface elevation, i.e. where the extension of wetted surface is varying in time, is cylindrical, while all other sections are either fully-submerged or fully-dry: the normals of a cylinder with vertical axis are horizontal, hence perpendicular to the heave direction, so they do no contribute to the build-up of the total heave force; it follows that the total vertical force depends on portions of the buoy that are always fully-submerged, hence not affected by improper definition of a mesh discretization. Conversely, surge and pitch forces depend also on the top cylinder, whose mesh quality influences the smoothness and accuracy of the results.

Finally, a synthetic but comprehensive view on the differences between linear and nonlinear excitation force coefficient is provided in Fig. 8, where $\hat{F}_{ex}$ is defined as the ratio between the force and the wave height: in a linear case, all curves should overlap, while differences may arise as nonlinearities increase. In the plot, both the amplitude and the mean are presented, where the amplitude is defined as the semi-difference between peak and trough. In the linear case, the amplitude is the same as the peak value, while the mean is zero. Figure 8 shows that, as H_w increases (colour code), the mean diverges from zero, especially in heave. Conversely, differences in the amplitude seem negligible.

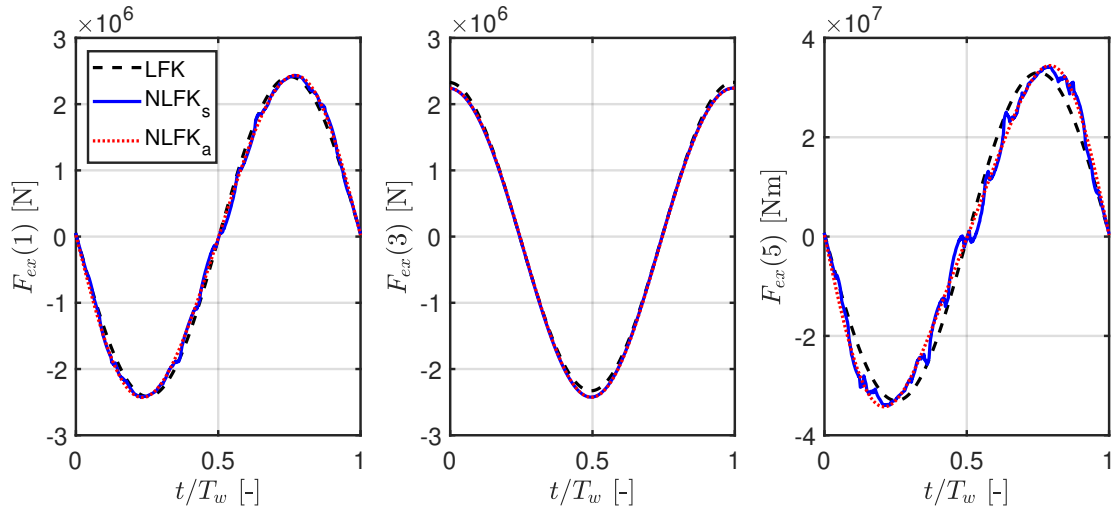

Fig. 7. Time trace over a single wave period of the total excitation force at T_w of 14 s and H_w of 4 m.

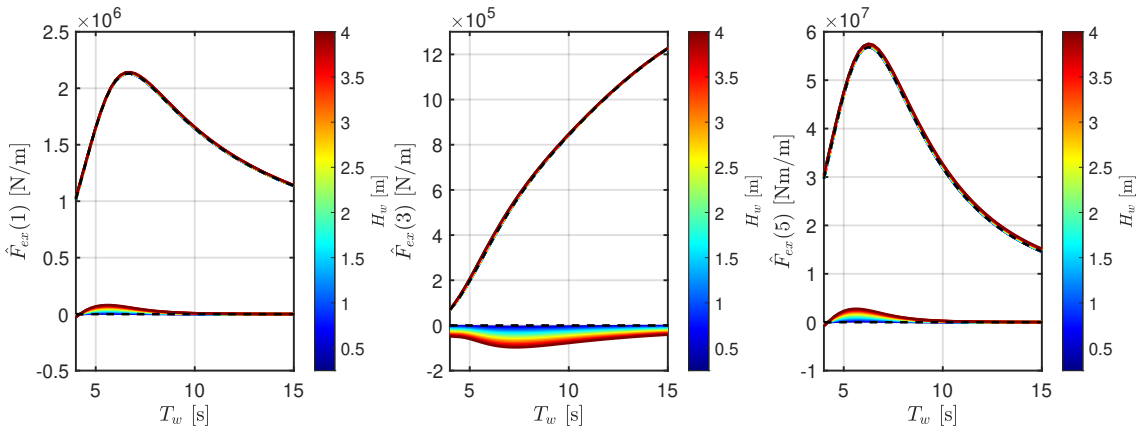

Fig. 8. Amplitude and mean values of the nonlinear excitation force at different wave heights. Dashed line corresponds to the linear case.

IV. Conclusions

This paper implements two alternative methods for the computation of nonlinear Froude-Krylov forces, one using a mesh-based approach in the popular WEC-Sim software, the other using a mesh-less analytical formulation of the wetted surface and numerical integration. As a case study, the Spar-buoy floating oscillating water column is used. An overall good agreement is found between the two alternative methods, cross-checking the underlying mathematical frameworks and implementations. However, the mesh-based approach shows inaccuracies in surge and pitch force computation, likely due to an improper selection of the mesh discretization. The computational time, although depending on various parameters and simulation setups, appear to be in favour of the analytical formulation (twice as fast as the mesh-based approach), despite of a complex shape definition, also providing accurate and smooth results.

In the future, this trends should be evaluated with a more thorough sensitivity analysis for the mesh and incorporating the dynamics of floating buoys with, at least, 3 degrees-of-freedom.

Acknowledgement

This research has received funding from the European Research Council (ERC) under the European Union's Horizon 2020 research and innovation program under Grant No. 832140.

References

[1] M. Penalba, G. Giorgi, and J. V. Ringwood, "Mathematical modelling of wave energy converters: a review of nonlinear approaches," *Renewable and Sustainable Energy Reviews*, vol. 78, pp. 1188–1207, 2017.

[2] Y.-H. Yu, K. Ruehl, J. V. Rij, N. Tom, D. Forbush, D. Ogden, A. Keester, and J. Leon, "WEC-Sim v4.2," 2020.

[3] J. Ringwood, F. Ferri, N. Tom, K. Ruehl, N. Faedo, G. Bacelli, Y. H. Yu, and R. G. Coe, "The wave energy converter control competition: Overview," in *Proceedings of the International Conference on Offshore Mechanics and Arctic Engineering - OMAE*, vol. 10. American Society of Mechanical Engineers (ASME), nov 2019. [Online]. Available: http://asmedigitalcollection.asme.org/OMAE/proceedings-pdf/OMAE2019/58899/V010T09A035/6444644/v010t09a035-omae2019-95216.pdf

[4] S. Sirnivas, Y. H. Yu, M. Hall, and B. Bosma, "Coupled mooring analyses for the wec-sim wave energy converter design tool," in *Proceedings of the International Conference on Offshore Mechanics and Arctic Engineering - OMAE*, vol. 6. American Society of Mechanical Engineers (ASME), oct 2016. [Online]. Available: http://asmedigitalcollection.asme.org/OMAE/proceedings-pdf/OMAE2016/49972/V006T09A023/2570062/v006t09a023-omae2016-54789.pdf

[5] Y. H. Yu, N. Tom, and D. Jenne, "Numerical analysis on hydraulic power take-off for wave energy converter and power smoothing methods," in *Proceedings of the International Conference on Offshore Mechanics and Arctic Engineering - OMAE*, vol. 10. American Society of Mechanical Engineers (ASME), sep 2018. [Online]. Available: http://asmedigitalcollection.asme.org/OMAE/proceedings-pdf/OMAE2018/51319/V010T09A043/2536992/v010t09a043-omae2018-78176.pdf

[6] J. Van Rij, Y. H. Yu, and R. G. Coe, "Design load analysis for wave energy converters," *Proceedings of the International Conference on Offshore Mechanics and Arctic Engineering - OMAE*, vol. 10, no. November 2019, 2018.

[7] A. Mérigaud, J.-C. Gilloteaux, and J. V. Ringwood, "A nonlinear extension for linear boundary element methods in wave energy device modelling," in *ASME 2012 31st International Conference on Ocean, Offshore and Arctic Engineering*, Rio de Janeiro, 2012, pp. 615–621. [Online]. Available: http://proceedings.asmedigitalcollection.asme.org/proceeding.aspx?doi=10.1115/OMAE2012-83581

[8] G. Giorgi and J. V. Ringwood, "Analytical representation of nonlinear Froude-Krylov forces for 3-DoF point absorbing wave energy devices," *Ocean Engineering*, vol. 164, no. 2018, pp. 749–759, 2018.

[9] H. Wang, A. Somayajula, J. Falzarano, and Z. Xie, "Development of a Blended Time-Domain Program for Predicting the Motions of a Wave Energy Structure," *Journal of Marine Science and Engineering*, vol. 8, no. 1, p. 1, dec 2019.

[10] G. Giorgi, R. P. F. Gomes, G. Bracco, and G. Mattiazzo, "Numerical investigation of parametric resonance due to hydrodynamic coupling in a realistic wave energy converter," *Nonlinear Dynamics*, 2020.

[11] K. R. Tarrant and C. Meskell, "Investigation on parametrically excited motions of point absorbers in regular waves," *Ocean Engineering*, vol. 111, pp. 67–81, 2016.

[12] G. Giorgi, R. P. F. Gomes, G. Bracco, and G. Mattiazzo, "The effect of mooring line parameters in inducing parametric resonance on the Spar-buoy oscillating water column wave energy converter," *Journal of Marine Science and Engineering*, vol. 8, no. 1, pp. 1–20, jan 2020.

[13] M. Penalba, A. Mérigaud, J. C. Gilloteaux, and J. V. Ringwood, "Influence of nonlinear Froude–Krylov forces on the performance of two wave energy points absorbers," *Journal of Ocean Engineering and Marine Energy*, vol. 3, no. 3, pp. 209–220, 2017.

[14] C. Windt, N. Faedo, M. Penalba, F. Dias, and J. V. Ringwood, "Reactive control of wave energy devices – the modelling paradox," *Applied Ocean Research*, vol. 109, p. 102574, 2021. [Online]. Available: https://www.sciencedirect.com/science/article/pii/S0141118721000511

[15] J.-C. Gilloteaux, "Mouvements de grande amplitude d'un corps flottant en fluide parfait. Application á la recuperation de l'energie des vagues," Ph.D. dissertation, Ecole Centrale de Nantes-ECN, 2007.

[16] M. Lawson, Y. H. Yu, A. Nelessen, K. Ruehl, and C. Michelen, "Implementing nonlinear buoyancy and excitation forces in the WEC-SIM wave energy converter modeling tool," in *Proceedings of the International Conference on Offshore Mechanics and Arctic Engineering - OMAE*, vol. 9B. American Society of Mechanical Engineers (ASME), oct 2014. [Online]. Available: http://asmedigitalcollection.asme.org/OMAE/proceedings-pdf/OMAE2014/45547/V09BT09A043/4432906/v09bt09a043-omae2014-24445.pdf

[17] G. Giorgi and J. V. Ringwood, "Comparing nonlinear hydrodynamic forces in heaving point absorbers and oscillating wave surge converters," *Journal of Ocean Engineering and Marine Energy*, vol. 4, no. 1, pp. 25–35, 2018.

[18] A. Mérigaud and J. V. Ringwood, "A nonlinear frequency-domain approach for numerical simulation of wave energy converters," *IEEE Transactions on Sustainable Energy*, vol. 9, no. 1, pp. 86–94, 2018.

[19] G. Giorgi, "Nonlinear Froude-Krylov Matlab demonstration toolbox," 2019.

[20] G. Giorgi, R. P. Gomes, J. C. Henriques, L. M. Gato, G. Bracco, and G. Mattiazzo, "Detecting parametric resonance in a floating oscillating water column device for wave energy conversion: Numerical simulations and validation with physical model tests," *Applied Energy*, vol. 276, oct 2020.

[21] R. Gomes, J. Henriques, L. Gato, and A. Falcão, "Time-domain simulation of a slack-moored floating oscillating water column and validation with physical model tests," *Renewable Energy*, vol. 149, pp. 165–180, apr 2020.

[22] G. Rinaldi, J. C. Portillo, F. Khalid, J. C. Henriques, P. R. Thies, L. M. Gato, and L. Johanning, "Multivariate analysis of the reliability, availability, and maintainability characterizations of a Spar–Buoy wave energy converter farm," *Journal of Ocean Engineering and Marine Energy*, vol. 4, no. 3, pp. 199–215, aug 2018. [Online]. Available: https://doi.org/10.1007/s40722-018-0116-z

[23] F. Correia da Fonseca, R. Gomes, J. Henriques, L. Gato, and A. Falcão, "Model testing of an oscillating water column spar-buoy wave energy converter isolated and in array: Motions and mooring forces," *Energy*, vol. 112, pp. 1207–1218, 2016.

[24] G. Giorgi and J. V. Ringwood, "Relevance of pressure field accuracy for nonlinear Froude–Krylov force calculations for wave energy devices," *Journal of Ocean Engineering and Marine Energy*, vol. 4, no. 1, pp. 57–71, 2018.

[25] I. WAMIT, "WAMIT User Manual," 2019.

[26] L. F. Shampine, "Matlab program for quadrature in 2D," *Applied Mathematics and Computation*, vol. 202, no. 1, pp. 266–274, 2008.